ELSEVIER

International Journal of Heat and Fluid Flow 23 (2002) 36–51

International Journal of HEAT AND FLUID FLOW

www.elsevier.com/locate/ijhff

Turbulent pipe flow of thixotropic fluids

A.S. Pereira [a], F.T. Pinho [b,*]

[a] *Departamento de Engenharia Química, Instituto Superior de Engenharia do Porto, Rua Dr. António Bernardino de Almeida 431, 4020-072 Porto, Portugal*

[b] *Centro de Estudos de Fenómenos de Transporte, DEMEGI, Faculdade de Engenharia, Universidade do Porto, Rua Roberto Frias, 4200-465 Porto, Portugal*

Received 19 January 2001; accepted 29 July 2001

Abstract

In this work, aqueous suspensions of 1% and 1.5% by weight laponite and a blend of 0.5%/0.07% laponite/carboxymethil cellulose (CMC) are investigated in terms of their rheology and hydrodynamic behaviour in pipe flows. All fluids were shear-thinning, thixotropic and had an yield stress which was measured by direct and indirect methods. The oscillatory tests showed that the 1% laponite suspension was inelastic but the other two fluids exhibited some degree of elasticity. The turbulent pipe flow measurements showed a small amount of drag reduction for the pure laponite suspensions, which was basically accounted for by shear-thinning at Reynolds numbers in excess of 35,000, whereas for the polymer–clay blend the drag reduction was significantly more intense. This work confirmed findings in the literature that the equilibrium condition in the pipe flow was different from the equilibrium condition in the flow curve, which caused some difficulties in data interpretation. However, it found negligible drag reduction for the flow of pure 1.5% laponite suspensions at Reynolds numbers in excess of 60,000, in contradiction to previous findings.

Keywords: Thixotropy; Turbulent pipe flow; Laponite suspension; Laponite–CMC blend; Drag reduction

1. Introduction

Drilling fluids have to fulfil a multitude of tasks, such as lubricating and cooling the drillbit, carrying the suspended rock cuttings to the surface, and pressurise the well in order to avoid well-collapse, amongst others. To accomplish these diverse tasks the fluids contain various additives, such as polymer molecules and clay particles, that impart a complex rheological behaviour characterised by variable viscosity, viscoelasticity, yield stress and thixotropy (see, for instance, Alderman et al., 1988; Lockett, 1992). One clay that is used sometimes as an additive in drilling muds is laponite, which has the advantage of transparency when suspended in water. It is a synthetic product which, alone or in combination with a polymer such as carboxymethil cellulose (CMC), produces fluids that have variable degrees of viscoelasticity, thixotropy, shear-thinning and viscoplasticity. These fluids are also very common in a wide variety of industrial situations, from the cosmetic and pharmaceutical industries to the cleaning, agriculture, building or paper industries to name but a few, and it is not surprising to find out that there are virtually hundreds of papers on their rheology (see the 20 years old review of Mewis, 1979). In some of these applications there is pumping of fluid in a pipe, very often under turbulent flow conditions.

The flow of these fluids is necessarily complex and still requires a significant amount of investigation to be better understood. Although there is a wealth of literature on the rheology of thixotropic fluids the same does not apply to the study of their pipe flow hydrodynamics. These fluids are usually opaque which severely limits the scope of experimental techniques to ultrasound devices, which lack spatial resolution for accurate measurements of turbulent flow, or to the new and promising, but still very expensive, nuclear magnetic resonance (see Iwamiya et al., 1994).

Therefore, it is no surprise to find only a few detailed research works involving non-Newtonian pipe flows of

* Corresponding author. Tel.: +351-225-081-762; fax: +351-225-081-763/445.

E-mail address: fpinho@fe.up.pt (F.T. Pinho).

0142-727X/02/$ - see front matter
PII: S0142-727X(01)00131-X

Nomenclature

D	pipe diameter (m)
DR	total drag reduction, Eq. (6)
DR_v	purely viscous drag reduction, Eq. (7)
f	Darcy friction factor, Eqs. (3), (5), (8) and (9)
f_N	Darcy friction factor for a Newtonian fluid, Eqs. (6), (7) and (10)
f_{st}	Darcy friction factor for a shear-thinning fluid, Eqs. (7) and (10)
G'	storage modulus (Pa)
G''	loss modulus (Pa)
K	consistency index in Herschel–Bulkley model (Pa s)^n, Eq. (1)
n	power index in power law or Herschel–Bulkley model
r	radial position
R	pipe radius
Re_w	Reynolds number based on the viscosity at the wall shear rate
t	time (s)
u	axial velocity
u'	rms of the instantaneous axial velocity (m/s)
u^+	axial velocity in wall co-ordinates (m/s)
u^*	friction velocity (m/s)
U	bulk velocity (m/s)
U_0	centreline velocity (m/s)
v'	rms of the instantaneous radial velocity (m/s)
y^+	distance from pipe wall in wall co-ordinates
w'	rms of the instantaneous tangential velocity (m/s)
$\langle\varepsilon\rangle$	area-average rate of dissipation of turbulent kinetic energy, Eq. (11)
Δf_N	uncertainty in Newtonian friction factor, Eq. (10)
ΔDR_v	uncertainty in the purely viscous drag reduction, Eq. (10)
γ	shear deformation
$\dot{\gamma}$	shear rate (s^{-1})
η	viscosity (Pa s)
η_w	viscosity at the wall shear rate (Pa s)
η_∞	viscosity parameter in Casson model (Pa s), Eq. (2)
ρ	density (kg/m^3)
τ	shear stress (Pa)
τ_c	yield stress measured in the creep test (Pa)
τ_{Cas}	yield stress in Casson model (Pa), Eq. (2)
τ_{HB}	yield stress in Herschel–Bulkley model (Pa) Eq. (1)
τ_s	yield stress measured in the increasing stress test of API (Pa)
τ_w	wall shear stress (Pa)

very fine, homogeneous suspensions under turbulent flow conditions. Some such works are the LDA measurements of Park et al. (1989) with an oil-based transparent slurry with yield stress obeying the Herschel–Bulkley law and the more recent investigations of Escudier et al. (1992, 1996). Escudier and Presti (1996) and Escudier et al. (1992) used transparent aqueous suspensions based on laponite and a mixture of laponite and a polymer, respectively. Park et al. used silica particles suspended in a mixture of Stoddard solvent and mineral oil and reported on a time-independent, yield stress fluid following theory in laminar flow and a behaviour similar to that of Laufer (1954) in the turbulent flow regime. Laponite suspensions in water are considered as model fluids in various types of rheological and hydrodynamic experiments because of their excellent clarity, non-toxicity and indefinite shelf life. These properties are due to their high purity, small particle size and incapacity to sustain bacterial growth (see Laponite, 1990a; Cocard et al., 2000).

A major difference between the two sets of works on pipe flow concerns the fluid rheology in respect to time dependence. For both cases, shear-thinning fluids with yield stress obeying the Herschel–Bulkley law were selected, but whereas in Park et al. the fluid was time independent, the laponite suspensions exhibited thixotropy. In Escudier and Presti (1996) the flow field was investigated in detail in the laminar, transitional and turbulent flow regimes. They could only predict accurately the laminar pipe flow with the Herschel–Bulkley model fitted to the velocity profiles, i.e., indirectly to the viscosity data at the prevailing flow conditions, rather than to the equilibrium state viscosity data. They also found that the transitional Reynolds number was similar to that for Newtonian fluids. In turbulent flow the laponite suspensions exhibited drag reduction, but less than usually found in polymer solutions, and a lower transverse turbulence than that of the Newtonian flows. Suspensions based on laponite have been used in the annular flow experiments of Escudier et al. (1995a). There, a blend of laponite and CMC was used to investigate the rotating flow in a concentric annulus and the onset of Taylor instability.

Extensive research is still required to enhance our knowledge on the behaviour of fluids combining shear-thinning, viscoelasticity, thixotropy and yield stress in basic turbulent flows, such as the pipe or channel flows and that will benefit from research on the following topics:

1. assessing the effects of different types of rheological behaviour in isolation and in different combinations. In this respect much work has been done to characterise shear-thinning viscoelastic polymer solutions,

but the physics behind some of the more remarkable findings (say, drag reduction in turbulent pipe flow) and the development of effective predictive tools remains elusive;
2. analysing diameter/geometrical effects upon the flow hydrodynamics for the various types of fluid;
3. to characterise the yield stress behaviour of these fluids in different ways and to relate them to turbulent flow hydrodynamics. The existence of yield stress is controversial in a theoretical framework, although not from an engineering viewpoint. Its accurate measurement is not easy and many developments in instrumentation and procedures took place over the years, as exemplified by a small sample of papers (see, for instance, Charm, 1963; Keentok, 1982; Nguyen and Boger, 1983; Cheng, 1984). The accumulated experience has established a series of standard practices for carrying out the rheological testing of these fluids, as is reviewed in Nguyen and Boger (1992).

This is a very extensive research programme and it is very important that it be accomplished in a well thought way in order for the data to be consistent following, for instance, the example set by Escudier et al. (2001) on the reproducibility of the rheology of xanthan gum solutions.

The present paper contributes to the second and third objectives by characterising in detail and in different ways, the rheology of aqueous suspensions of laponite and a blend of laponite/CMC, after which measurements of pressure drop and mean and rms velocity profiles in turbulent pipe are presented. The pipe has a diameter of 26 mm and the diameter effect is investigated by comparing the results with those from the 100.8 mm diameter pipe of Escudier and Presti (1996).

The remaining of this report is organised as follows: first, the experimental facilities are described and this is followed by the rheological characterisation of the fluids. Pipe flow hydrodynamic results are investigated first on the basis of integral parameters after which detailed profiles of the mean and rms velocities are shown and discussed.

2. Experimental set-up and instrumentation

2.1. The rig, pressure transducers and flowmeter

The hydrodynamic measurements were carried out in the flow rig described in Pereira and Pinho (1994). Fluid was pumped from a 100 l tank through a rising pipe and then through the 90 diameter long descending pipe leading to the tank. The descending pipe had always a constant 26 mm inside diameter and consisted of a long vertical copper pipe, at the end of which stood the acrylic test section followed by the 900 mm long returning pipe. The transparent test section was 232 mm long and its outer cross-section was square in order to reduce refraction of laser beams.

The flow was controlled by two valves and one bypass circuit, and a 100 mm long star-shaped honeycomb was located at the inlet of the descending pipe to help ensure a fully developed flow in the test section. Heating and cooling circuits in the reservoir were used to control and maintain the temperature at a constant 25 ± 0.5 °C.

The test section had four pressure taps drilled, separated by a distance of 65 mm. Equal longitudinal pressure gradients measured in consecutive pairs of taps, and equal velocity profiles measured by LDA at the beginning and end of the test section confirmed a fully-developed flow situation.

The pressure drops were measured by means of two differential pressure transducers, models P305D-S20 and P305D-S24 from Valydine, and the flow rate was measured by an electromagnetic flowmeter Mag Master from ABB Taylor, which was incorporated in the rising pipe, 15 diameters downstream of the closest flow perturbation. All these instruments were connected to a 386 PC by a data acquisition Metrabyte DAS-8 board interfaced with a Metrabyte ISO4 multiplexer, both from Keithley.

The flowmeter was capable of measuring the volumetric flow rate in the range of 0–5 l/s with an accuracy of 0.2% of full scale. As a further check to its accuracy the velocity profile measurements carried out by LDA were integrated to yield a computed flowrate which never differed by more than 1% from the value read in the flowmeter.

As far as the uncertainty of the pressure measurements is concerned it is important to recall that these were carried out for fully developed flow, thus eliminating such sources of uncertainty as the hole pressure error of Novotny and Eckert (1973). All the pressure taps were drilled carefully to avoid the appearance of spurious edge effects and had the same geometry so that any systematic errors would cancel out in the pressure difference measurement. The recommendations of Shaw (1960) and Franklin and Wallace (1970) for the design of pressure taps and the quantification of pressure measurement errors were followed and it was estimated that the associated contribution to the overall uncertainty was less than 1.5% at a high Reynolds number. Taking into account the other sources of uncertainty, such as accuracy of the transducers, calibration errors, zero drift effects and statistics, the total uncertainty of the pressure difference measurements was estimated, by application of the root-mean square equation, to vary between 1.6% and 7.2% at high and low flow rates, respectively.

2.2. The laser-Doppler anemometer

A fibre optic laser-Doppler velocimeter from INVENT, model DFLDA, was used for the velocity

measurements with the 30 mm probe mounted on the optical unit. Scattered light was collected by a photo diode in the forward scatter mode, and the main characteristics of the anemometer are listed in Table 1 and described by Stieglmeier and Tropea (1992). The signal was processed by a TSI 1990C counter interfaced with a computer via a DOSTEK 1400 A card, which provided the statistical quantities. The data presented in this paper have not been corrected for the effects of the mean gradient broadening. The maximum uncertainties in the axial mean and rms velocities at a 95% confidence level are of 1% and 2.2% on axis, respectively, and of 1.3% and 5.2% in the wall region. The maximum uncertainty of the radial and tangential rms velocity components is 2.5% and 5.3% on axis and close to the wall, respectively.The refraction of the beams at the curved optical boundaries was taken into account in the calculations of the measuring volume location, measuring volume orientation and conversion factor, following the equations presented in Durst et al. (1981). For measurements of the radial component of the velocity, the plane of the laser beams was perpendicular to the test section axis and the anemometer was traversed sideways, in the normal direction relative to the optical axis.

The velocimeter was mounted on a milling table with movement in the three co-ordinates and the final positional uncertainties after corrections are those of Table 2. The positioning of the control volume was done visually with the help of infrared sensitive screens, video camera and monitor. Part of the systematic positional error was corrected by plotting the axial mean velocity profiles and, whenever the asymmetry of the flow was greater than half the size of the control volume, that value was added or subtracted to the milling table so that the profile became symmetric. This method was verified by measuring a second time the same velocity profile which was seen to be always symmetric after the correction was applied. Therefore, the final positional uncertainties are those associated with the precision of the measuring gauges and with the inherent limitations of the size of the measuring volume.

Table 1
Laser-Doppler characteristics

Laser wavelength	827 nm
Laser power	100 mW
Measured half angle of beams in air	3.68
Dimensions of measuring volume in water at e^{-2} intensity	
Minor axis	37 μm
Major axis	550 μm
Fringe spacing	6.44 μm
Frequency shift	2.5 MHz

Table 2
Estimates of positional uncertainty

Quantity	Bias (μm)	Random
x, y (horizontal plane) accuracy of milling table	±10	–
z (vertical) accuracy of milling table	±100	–
x, y (horizontal plane) accuracy of visual positioning	±200	–
z (vertical) accuracy of visual positioning	±100	–

2.3. The rheometer

The rheological characterisation of the fluids was carried out in a rheometer from Physica, model Rheolab MC 100, made up of an universal measurement unit UM/MC fitted with the low viscosity double-gap concentric cylinder Z1-DIN system. Following the recommendations of the manufacturer this geometry was adequate to measurements of these low viscosity suspensions because the gap size was more than 20 times the size of the larger particles (see Section 3.1 for information on particle size) and it allowed the measurement of viscosities between 1 mPa s and 67.4 mPa s at the maximum shear rate of 4031 s^{-1}. The rheometer could be both stress and shear rate controlled, a possibility that was used according to the ranges of viscosity and shear rate under observation. A thermostatic bath and temperature control system, Viscotherm VT, allowed the control of temperature of the fluid sample at 25 °C within 0.1 °C.

The rheometer was operated in steady-state to measure the viscometric viscosity, in oscillatory flow to measure the elastic and viscous components of the dynamic viscosity, and in creep tests to measure the yield stress. The creep test was also used in an attempt to quantify the fluid elasticity in the widest possible manner. In the viscometric viscosity measurements with the double gap concentric cylinder at low shear rates, the rheometer was operated in the controlled shear stress mode, and the uncertainty of the measurements was better than 3.5%, whereas at higher shear rates the shear rate control mode was used and the uncertainty was better than 2%. For the creep tests the uncertainty was better than 5% and 10% for high and low shear stresses, respectively.

3. Fluid characterisation

3.1. The fluids

The aqueous suspensions were based on the laponite RD clay manufactured by Laporte Industries. This laponite is a synthetic smectite clay with a structure analogous to the natural mineral clay hectorite, but with a smaller size. It is a layered hydrous magnesium silicate

which is hydrothermally synthetised from simple silicates and lithium and magnesium salts, in the presence of mineralising agents. Further details of the chemical structure of laponite, its production and applications can be found in Laponite (1990b).

Smectite clays swell as water, or polar organic solvents, enter the interlayer regions due to the hydration of the interlayer cations and the platelet surfaces. They have a structural negative charge due to the substitution of cations in the composite layers, which is independent of the level and type of electrolyte. Dilute suspensions of laponite in water with low electrolyte levels will remain as low viscosity "sols" of non-interacting individual platelets for long time periods. However, the electrolyte level and type has a marked effect on the stability and thickness of dispersed laponite particles. At concentrations higher than 3%, the whole solution gels as face to face interactions between the electrical double layers of individual platelets make them virtually immobile. This gives rise to an equilibrium structure with an elastic response to applied shear stress until a critical yield stress is exceeded. The most important feature of the rheology of the clay suspensions is its ability to form colourless, transparent, highly thixotropic gels (see Laponite, 1980). In the sols, the primary particles have a diameter of 250 Å and a thickness of 10 Å (see Laponite, 1990b).

Aqueous suspensions of 1% and 1.5% w/w of laponite RD and a blend of 0.5% laponite and 0.07% of CMC were produced for this work. The 1.5% suspension and the blend were selected to allow comparison with the works of Escudier et al. (1992, 1996). Blending laponite with CMC (sodium carboxymethyl cellulose) is suggested also by the manufacturer of laponite (see Laponite, 1979) as a way to increase the gel strength and its shear viscosity. However, the CMC utilised in this work (CMC grade 7H4C from Hercules with a molecular weight of 3×10^5 kg/kmol) was not the same as that used by Escudier et al. (1992, 1995a,b, 1996), who relied on a brand manufactured by Aldrich Chemical. A comparison between the rheology of both types of CMC at an identical weight concentration of 0.4% is presented in Escudier et al. (2001). Differences of about 25% are seen in the shear viscosity, with the Hercules grade being less viscous, but the storage and loss moduli in oscillating shear flow are practically the same.

All fluids were prepared with the same procedure using Porto tap water. To prevent bacteriological degradation 100 ppm of formaldehyde was added and 60 ppm of sodium chloride increased the yield stress of the solutions. More than 100 l of fluid were required to fill the pipe rig, and the solutions were mixed for 90 min and settled for more than 24 h to allow complete hydration of the intersticial spaces between the clay particles. Before the rheological characterisation of the suspensions and/or its transfer to the pipe flow rig the suspensions were mixed for 30 min to full homogenisation. All concentrations quoted in this work are weight concentrations.

3.2. Viscometric viscosity

All non-Newtonian fluids in this work are shear-thinning and have an yield stress and, because they are also thixotropic a flow-equilibrium test procedure had to be adopted to measure the viscometric viscosity. This procedure was established by Alderman et al. (1988) whereby a shear stress is applied to the fluid sample and the shear rate monitored until steady-state conditions are achieved after which the viscosity is taken. An example of such test is shown in Fig. 1 for the 1.5% laponite suspension. The upper curve represents the fluid response to a sudden increase in applied shear stress from 0 to 15 Pa whereas for the lower curve the stress was suddenly decreased from 35 Pa to 15 Pa. In both cases a steady-state situation prevailed for $t < 0$ s. According to some phenomenological models thixotropy is associated with an internal fluid structure within which a network of connections is continuously formed, as well as destroyed, by deformation (see Papenhuijzen, 1972). Thus, an equilibrium situation arises after some time as the rate of formation of internal connections equals its rate of destruction. The differences in both curves of Fig. 1 are related to the different initial equilibrium states at $t < 0$, but the response time is similar, of the order of 3000 s. This value is similar to that reported by Escudier and Presti (1996) for their 1.5% laponite suspension.

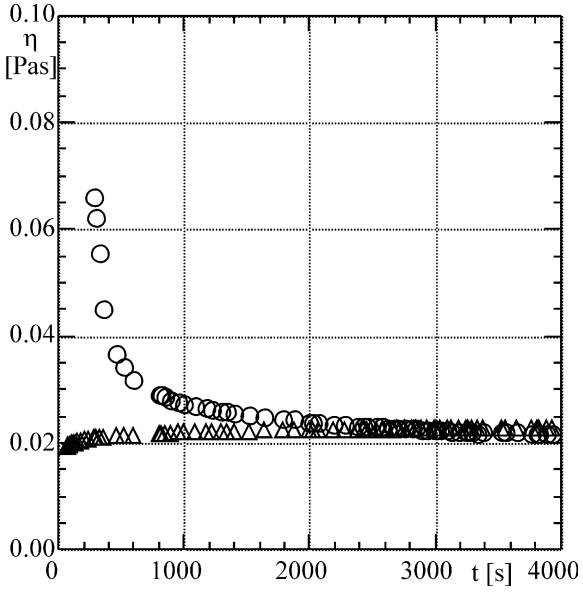

Fig. 1. Variation of the viscometric viscosity with time for a 1.5% laponite suspension. At $t = 0$ s a constant shear stress of 15 Pa is applied. (○) $\tau = 0$ Pa for $t < 0$ s; (△) $\tau = 35$ Pa for $t < 0$ s.

Repeating this procedure the viscosity curves of Fig. 2 are obtained which correspond to the final equilibrium states for a wide range of shear stresses/shear rates for all fluids. The suspensions of laponite exhibit an increase of the viscosity with concentration and a strong shear-thinning behaviour without the Newtonian plateau at low shear rates, as is typical of fluids possessing an yield stress. At high shear rates the viscosities are rather low, just of the order of five times the viscosity of the solvent, even for the more concentrated suspensions.

Fig. 2 includes the viscosities of a suspension of pure laponite at a concentration of 0.5% as well as of a solution of pure CMC at a concentration of 0.07%. These two fluids have viscosities 5 to 10 times lower than the viscosity of the 0.5% laponite/ 0.07% CMC blend for shear rates between 10 and 1000 s^{-1}. The 0.07% CMC solution is clearly thicker than the 0.5% laponite suspension, and the evolution of the latter at low shear rates suggests that it also possesses an yield stress. The synergetic effect of the blend is clearly shown in the corresponding viscosity which has values similar to the viscosity of the pure 1.5% laponite suspension with only about a third of the total amount of additives. Based on a single shear rate measurement, Laponite (1979) indicated this possibility.

The viscosity data were fitted by the Herschel–Bulkley model of Eq. (1), which resulted in the parameters listed in Table 3 and are represented by the solid lines in Fig. 2. The dashed line pertains to the Herschel–Bulkley model fitted to the viscosity data of the 1.5% suspension

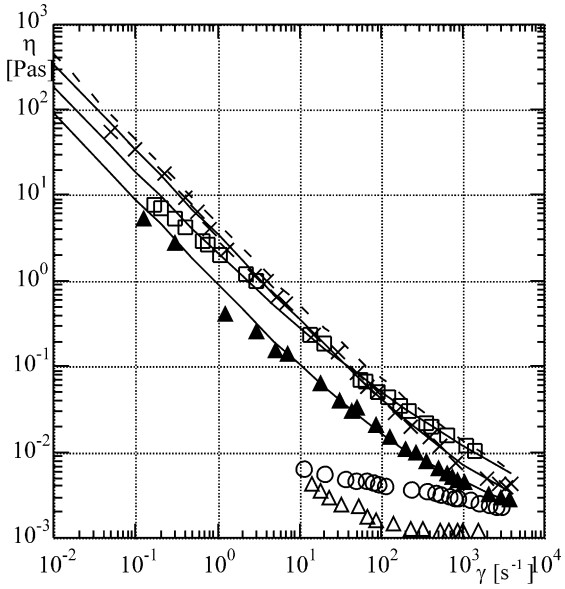

Fig. 2. Viscometric viscosity of all suspensions in the equilibrium state. (○) 0.07% CMC; (△) 0.5% laponite; (□) 0.5%/0.07% laponite/CMC; (▲) 1% laponite; (×) 1.5% laponite; full lines represent fitting by the Herschel–Bulkley model. Dashed line represents the fitted Herschel–Bulkley model to 1.5% laponite data from Escudier and Presti (1996).

Table 3
Parameters of the Herschel–Bulkley stress model fitted to the viscosity data

Solutions	n	K (Pa s^n)	τ_{HB} (Pa)
0.5%/0.07% laponite/CMC	0.492	0.347	1.8
1% laponite	0.685	0.033	0.9
1.5% laponite	0.676	0.037	3.4
1.5% laponite from EP	0.535	0.240	4.4

Includes data from EP: Escudier and Presti (1996).

of Escudier and Presti (1996). The viscosity of their suspension was higher than that of our corresponding fluid for reasons that will be explained later:

$$\eta = \frac{\tau_{HB}}{\dot{\gamma}} + K\dot{\gamma}^{n-1}. \quad (1)$$

3.3. Oscillatory shear flow

Measurements of the storage (G') and loss (G'') moduli in oscillatory shear flow were carried out for all fluids, but the maximum shear amplitude for linear behaviour was so small that accurate results were difficult to obtain, especially with the more dilute fluids.

For the 1% and 1.5% laponite suspensions the fluid elasticity was lower than for the laponite/CMC blend at high frequencies as can be assessed in Table 4 which lists typical values of the ratio G'/G'' in two frequency ranges. As assessed by this test the elasticity of the 1.5% laponite suspension and of the blend was higher than that of dilute tylose and CMC solutions tested by Coelho and Pinho (1998) and of the dilute xanthan gum solutions of Pereira and Pinho (1999); the ratio G''/G'' of the 1% laponite suspension was rather small. Again, the synergetic effect of the polymer–clay blend is well shown in that G''/G'' is similar to that of the 1.5% suspension containing three times more additives but no

Table 4
Typical ratio between the storage and loss moduli at two ranges of frequency

Solution	G''/G''	
	Frequency	
	1–5	5–10
1% laponite	0.12	0.14
1.5% laponite	3.1	1.7
0.5/0.07 lap/CMC	2.9	1.9
0.6% tylose from Coelho and Pinho (1998)		0.3
0.4% CMC from Coelho and Pinho (1998)		0.6
0.25% XG from Pereira (2000)		0.7

polymer. This is certainly due to the reinforcement of the internal structure of solid particles by the polymer molecules (see Boger, 1994).

3.4. Yield stress

The yield stress of a fluid is intimately related to the bond forces within the structure of the suspension and therefore it is a measure of the force required to break that structure when it is fully formed and under a static condition. For stresses higher than the yield stress the internal structure of the fluid has been destroyed, but in other cases it continues to exist in a state of dynamic equilibrium in which case internal connections are permanently being formed and destroyed. In this latter case the behaviour of the fluid becomes time dependent, i.e., thixotropy sets in and there is an association of viscoplastic and thixotropic behaviour.

According to Cheng (1986), the yield stress is also sensitive to the duration and type of test procedure and especially so for time-dependent fluids as in this work. The yield stress was obtained here using some of the direct and indirect procedures described by Nguyen and Boger (1992). The direct techniques were the creep test and the increasing stress test defined by the American Petroleum Institute (API), whereas the indirect methods were the extrapolation of the equilibrium viscosity data by known rheological models. The final results will now be presented here together with a brief description of individual results.

In the creep test increasing values of the shear stress were applied to the fluid sample for a period of time and then the stress was removed. When the applied stress was higher than the yield stress there was a final deformation at the end of the experiment. The test is exemplified in Fig. 3 which presents typical deformation curves for different applied stresses when the fluid sample was the 1% laponite suspension. For stresses of 0.6 and 1.5 Pa there was no residual deformation, for 1.75 Pa there was a very small residual deformation of $\gamma = 0.1$ and for an applied stress of 1.9 Pa the fluid had clearly yielded. So, yielding did not occur abruptly but started just under 1.75 Pa and was complete for 1.9 Pa.

In the increasing stress test of API (see Speers et al., 1987) the yield stress was the maximum stress value identified by Pryce-Jones (1952) and Papenhuijzen (1972) which, according to the more recent interpretation of Liddell and Boger (1996), corresponds to the stress marking the transition between the viscoelastic and purely viscous behaviour. However, the time resolution of our rheometer was not sufficient for a clear maximum stress to be observed and consequently the results from this test (τ_s) should be regarded with caution.

In the indirect methods the equilibrium viscosity sets containing 23 data points were fitted by two typical

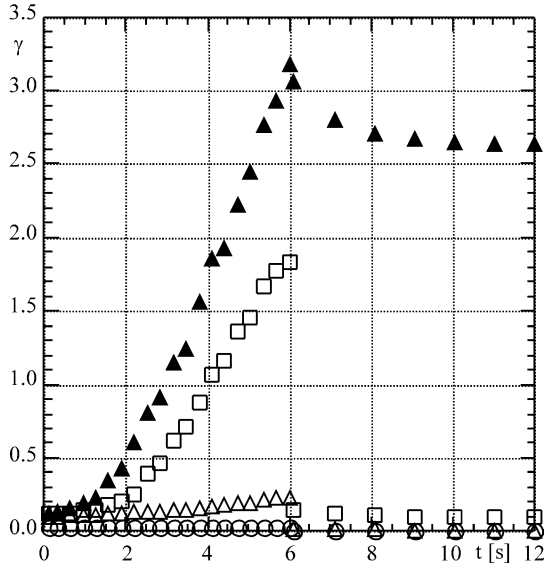

Fig. 3. Variation of sample deformation with time in a creep test for the determination of the yield stress for the 1% laponite suspension: (○) $\tau = 0.6$ Pa; (△) $\tau = 1.5$ Pa; (□) $\tau = 1.75$ Pa; (▲) $\tau = 1.9$ Pa.

rheological equations, the Casson model Eq. (2) of Casson (1959) and the Herschel–Bulkley model Eq. (1), the latter shown by the solid lines in Fig. 2:

$$\eta = \frac{\tau}{\dot{\gamma}} \quad \text{with} \quad \sqrt{\tau} = \sqrt{\tau_{\text{Cas}}} + \sqrt{\eta_\infty \dot{\gamma}}. \tag{2}$$

The Herschel–Bulkley and Casson models are purely empirical equations derived in 1926 and 1959, respectively, to relate the shear stress and shear rate for materials that flow when the stress exceeds a critical value, the so-called yield stress. The Herschel–Bulkley equation is an extension of the power law model of Ostwald-de-Waele to deal with yield stress fluids, but for this purpose it requires three numerical parameters. On the contrary, the Casson equation can fit adequately many real yield stress fluids, often with less accuracy, such as printing inks (Casson, 1959) and blood (Shah, 1980), simply with two parameters. More information on rheology and constitutive equations can be found in Barnes et al. (1989) and Barnes (2000).

Except for the blend, where a difference in excess of 20% was found, the two fittings resulted in similar yield stress values. This can be seen in Table 5, which

Table 5
Yield stress values obtained by the various methods

Solution	τ_c	τ_s	τ_{Cas}	τ_{HB}
Lap 0.5%/0.07% CMC	2.2	2.3	2.3	1.8
laponite 1%	1.8	1.7	0.8	0.9
laponite 1.5%	5.8	4.8	3.3	3.4

τ_c: creep; τ_s: increasing stress; τ_{Cas}: Casson model fitting; τ_{HB}: Herschel–Bulkley model fitting.

compares and summarises the results of the various direct and indirect measurements of the yield stress. Similar yield stress values resulted from fitting the data by polynomials of the fourth- and fifth-order or by averaging the asymptotic values of the shear stress at low shear rates, and here we must bear in mind the high measuring uncertainties at low shear rates. For the blend, careful inspection of the data showed a less well defined asymptotic behaviour at low shear rates and more scatter.

The comparison between the two direct measurements of the yield stress in Table 5 shows fair agreement for the 1% suspension and the blend, whereas a difference of less than 20% is seen for the 1.5% laponite suspension. However, as mentioned above, the increasing stress method is less reliable here because of the limitations of our rheometer.

The values of stress obtained by the different measuring techniques must necessarily be different: whereas the creep test measures the yield stress without destroying the inner structure of the fluid sample, the indirect measurements rely on a procedure that requires a different, less ordered state of dynamic equilibrium. In all cases the yield stress increases with additive concentration and the difference between the values obtained by direct and indirect methods depends on the fluid: of the order of 20% for the blend but by a factor of 2 for the pure suspensions, with the indirect methods always resulting in lower values.

From a critical assessment of the set of results one may conclude that the yield stress values of relevance to the hydrodynamic results are those obtained from dynamic equilibrium experiments, i.e., the indirect values, and those obtained with the Herschel–Bulkley rheological model are preferred. These are 0.9, 2.1 and 3.4 Pa for the 1% laponite suspension, the 0.5%/0.07% laponite/CMC blend and the 1.5% laponite suspension, respectively. For the 1.5% laponite suspension Escudier and Presti (1996) obtained a yield stress of 4.4 Pa using the Herschel–Bulkley fitting. A comparison of the viscosities of both 1.5% suspensions shows theirs to be slightly thicker. This difference could be attributed to ageing; Escudier and Presti (EP) state that their fluid was used one week after preparation and that they observed, as confirmed by the manufacturer and by Cocard et al. (2000), that the laponite suspensions thicken with time, whereas in our case the fluid was used within a couple of days.

4. Results and discussion

4.1. Initial considerations

Before presenting the results of the measurements it is advantageous to define and present some quantities for conciseness. Back in 1959, Dodge and Metzner derived an expression for the friction factor of purely viscous, shear rate-dependent fluids. It can be argued whether the fluids they used to obtain the parameters of the expression were purely viscous, but that is still the best model available for such class of fluids and, even if they were not purely viscous they must have been pretty close to that. Dodge and Metzner's equation is cast here in terms of the Darcy friction factor

$$f \equiv \frac{8\tau_w}{\rho U^2} \tag{3}$$

and the wall Reynolds number

$$Re_w \equiv \frac{\rho UD}{\eta_w} \tag{4}$$

as

$$\frac{1}{\sqrt{f}} = 0.8685n^{0.25}\ln\left(\frac{2n}{3n+1}Re_w\sqrt{f}\right) + \frac{2.4082}{n^{0.75}}(1-n) - \frac{0.2}{n^{1.2}}, \tag{5}$$

where U is the bulk velocity, D is the pipe diameter, ρ is the fluid density, n is the power law exponent and τ_w and η_w are the shear stress and viscosity at the wall shear rate, respectively.

Dodge and Metzner (1959) equation is usually represented as a function of the generalised Reynolds number (Re_{gen}) which was defined on the basis of laminar flow considerations. In that classical representation of the friction factor there is drag reduction with increasing shear-thinning, with a fairly constant variation in $\log(f)$ with the variation in n, at constant generalised Reynolds numbers.

The use of a Reynolds number based on the wall viscosity is more adequate for turbulent flow because it is in the wall region that viscous stresses play a dominant role. In this alternative plot, which is shown in Fig. 4, shear-thinning is again responsible for drag reduction so that, for a fluid with, say $n < 0.5$, drag reductions in excess of 20% are predicted at constant wall Reynolds numbers. However, for the same value of the power index and Reynolds number the variations in f due to shear-thinning are significantly less when using the wall viscosity than with the apparent viscosity that appears in the generalised Reynolds number of Dodge and Metzner.

It is convenient to define here what is meant by drag reduction. We use the definition

$$\mathrm{DR} \equiv \frac{f_N - f}{f_N} \times 100 \tag{6}$$

with all quantities obtained at the same wall Reynolds number: f represents the value of the measured friction factor for any fluid and f_N the corresponding Newtonian coefficient at the same Reynolds number. Note that f_N is calculated from a power law fit to our experimental $f - Re$ water measurements data. Then, for any fluid the

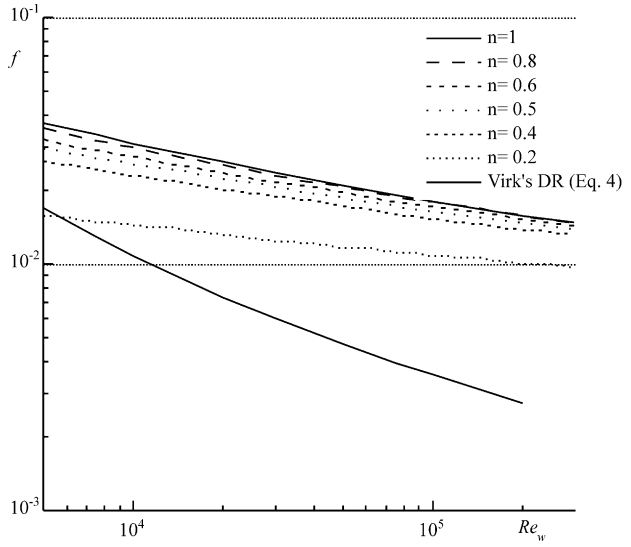

Fig. 4. Variation of the friction factor for purely viscous shear-thinning fluids Eq. (5) as a function of the wall Reynolds number, according to Dodge and Metzner (1959).

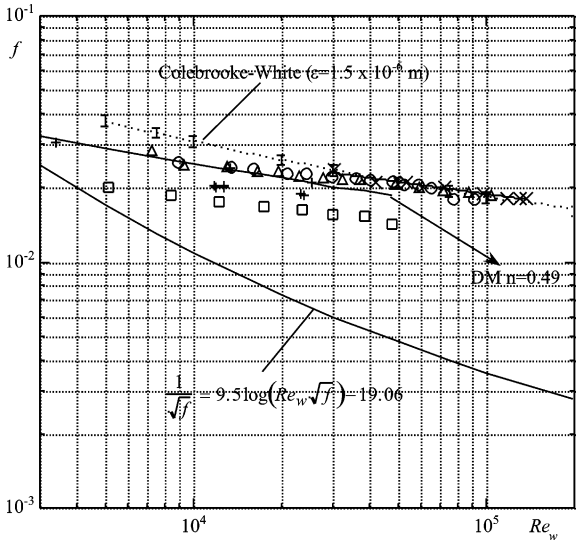

Fig. 5. Darcy friction factor as a function of the wall Reynolds number: (×) water; (□) 0.5%/0.07% laponite/CMC; (△) 1% laponite; (○) 1.5% laponite; (+) 1.5% laponite from Escudier and Presti (1996). Error bars in Colebrooke–White equation of ±5%.

total drag reduction DR can be decomposed into a purely viscous drag-reduction DR_v due to shear-thinning and a term accounting for other effects DR_e which is given by the difference $DR_e \equiv DR - DR_v$. The purely viscous drag reduction due to shear-thinning is calculated with Eq. (7) where $f_{st} = f$, as given by Dodge and Metzner's Eq. (5). Again, in Eq. (7) f_{st} and f_N pertain to the same Reynolds number based on the wall viscosity

$$DR_v = \frac{f_N - f_{st}}{f_N} \times 100. \tag{7}$$

4.2. Bulk flow characteristics

The bulk hydrodynamic behaviour of the various fluids is reported in Fig. 5 which plots the measured Darcy friction factor as a function of the wall Reynolds number. The viscosity at the wall was obtained from the measured shear stress and the equilibrium flow curve of the fluid. The upper dashed line in the figure represents the Colebrooke–White equation for a roughness of $\varepsilon = 1.5 \times 10^{-6}$ m which is a value more appropriate for smooth pipes (Geiringer, 1963) and the lower full curve is the maximum drag reduction asymptote with polymer solutions of Virk et al. (1970) given by

$$\frac{1}{\sqrt{f}} = 9.5 \log(Re_w \sqrt{f}) - 19.06. \tag{8}$$

The Newtonian data lies slightly above the Colebrooke–White equation for Reynolds numbers above 60,000, but the difference is small. However, since the Newtonian friction factor is used later as the reference to calculate the amount of drag reduction, the Newtonian data was fitted by a power law Blasius-type relationship which gave

$$f = 0.126 Re^{-0.1648} \tag{9}$$

and is also represented as a full line. To help in the comparisons, the purely viscous Eq. (5) for $n = 0.49$ was also represented as a full line and marked DM $n = 0.49$.

For all solutions a similar maximum bulk flow velocity in the range of 4.62–4.87 m/s was reached, but that corresponded to maximum Reynolds numbers of 137,000 for water and 104,000, 91,000 and 48,000 for the 1% and 1.5% laponite suspensions and the laponite/CMC blend, respectively. It should be emphasised that the pressure and flow rate measurements in the rig were only initiated after those quantities were observed to remain constant with time. The Newtonian data are consistent with previous results from various sources in the literature.

For Reynolds numbers below 30,000 the non-Newtonian fluids show drag reduction and especially so the laponite/CMC blend, whereas above 30,000 the friction factors of the pure laponite suspensions are very close to those of pure water. Eqs. (5)–(7) and (9) can now be used to quantify the amounts of total and shear-thinning drag reduction.

Under turbulent flow conditions the shear rates prevailing at the pipe wall are rather high, to which correspond shear stresses well above the yield stress. If we were to fit a power law viscosity model to the viscosity data at shear rates in the range of those encountered at the wall of a given pipe flow, the corresponding value of n could then be used to predict the purely viscous friction factor using Eq. (5) and hence the amount of

viscous drag reduction DR_v by means of Eq. (7). This process is rather cumbersome as it implies a different viscosity fit for each flow condition. Since under turbulent flow conditions the wall shear stresses are significantly higher than the yield stress, the power index n of the Herschel–Bulkley fit (in Table 3) is close to, but lower than, the value that would be obtained through the dedicated power law fit described above. Its use, thus, provides a sufficiently accurate estimate of DR_v which, at most, is slightly over-predicted.

The drag reduction intensities are plotted in Fig. 6 as a function of the wall Reynolds number. The largest drag reduction as well as the largest difference $DR - DR_v$ is that of the clay–polymer blend, certainly due to the synergetic effect of the polymer on the clay. Both suspensions of pure clay have viscous drag reductions going down from 8% at $Re = 10,000$ to about 5% at $Re = 50,000$ and increasing to 7% at $Re = 100,000$. This non-monotonic variation results from using the Colebrooke–White correlation and the Blasius-type Eq. (9) to calculate the Newtonian friction factor f_N appearing in Eqs. (6) and (7) for Reynolds number below and above 50,000, respectively. The reader should be aware of the high uncertainty in DR_v whose maximum absolute value is represented on the left lower corner of the figure. That maximum uncertainty ΔDR_v is calculated using the root-mean square rule and Eq. (7):

$$\Delta DR_v = \frac{dDR_v}{df_N}\Delta f_N = 100\frac{\Delta f_N}{f_N}\frac{f_{st}}{f_N} \tag{10}$$

and assuming an average value of $\Delta f_N/f_N \approx 0.05$ taken from Section 2.1.

The drag reduction tends to vanish at high Reynolds numbers for the pure suspensions and, at $Re_w \approx 35,000$, there is even a crossover of the total (DR) and viscous (DR_v) drag reductions, an indication of an anomalous behaviour. For the 1.5% laponite suspension there is also some scatter of the data, the outcome of a small difference between two large numbers. As will be shown later, the crossover most likely results from an overestimation of the purely viscous drag reduction.

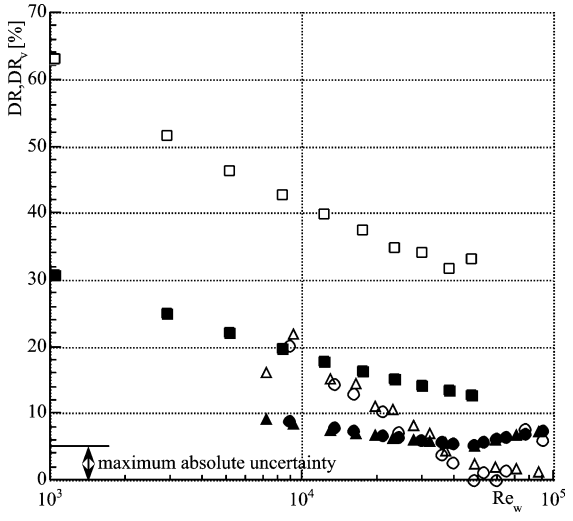

Fig. 6. Drag reduction intensity: (□) 0.5%/0.07% laponite/CMC; (△) 1% laponite; (○) 1.5% laponite. Open symbols: total drag reduction DR; closed symbols: shear-thinning drag reduction DR_v.

At this stage it is worth comparing our results with the data of Escudier and Presti (1996) for the 1.5% laponite suspension and to look carefully at their findings. We have seen in Fig. 2 that, although their 1.5% laponite suspension was more viscous than ours, the variation of viscosity with shear rate in log–log coordinates was parallel, i.e., their power index had basically the same numerical value which implies the same amount of viscous drag reduction according to Eq. (5). In Fig. 5, their friction factors are intermediate to ours for pure laponite and the laponite/CMC blend and exhibit a clear drag reduction, far in excess of the purely viscous effect and this is a different result from ours. Their maximum Reynolds number is well below 35,000, which marks the crossover of DR and DR_v in our data.

The high spatial resolution of their LDA velocity measurements allowed them to measure velocities within the laminar sublayer from which they could determine the true wall shear rate, and their pressure drop measurements quantified the true wall shear stress. Escudier and Presti found that, for the same wall shear stress, the shear rate determined from the sublayer velocity profile was lower than that determined from the equilibrium flow curve, a situation arising from the fluid thixotropy and leading to a higher wall viscosity than estimated from the rheogram. This was attributed to different equilibrium conditions of the laponite suspension in the pipe rig and in the rheometer.

In our rig the diameter of the pipe is four times smaller than in Escudier and Presti ($D_{EP} = 4D$) and the length of our pipe is also shorter by a factor of more than five (say $L_{EP} \approx 5L$). Comparing the viscosities of our 1.5% laponite suspension with that of Escudier and Presti (EP) in Fig. 2, we also find that at high shear rates $\eta_{EP} \approx 2\eta$. Now, for identical Reynolds numbers we determine $U_{EP} \approx 0.5U$, where U refers to bulk velocity and the transit time of the fluid in the rig can be estimated as $T = L/U$, which gives $T_{EP} = 10$ T, i.e., in our rig it will be shorter than in Escudier and Presti's. So, due to fluid thixotropy the equilibrium condition in our pipe flow rig must be further away from the equilibrium condition of the flow curve than was the case in their experiments.

The difference is not simply a matter of comparing transit times because the equilibrium between the formation and rupture of internal connections of the fluids also depends on the local intensities of the turbulent flow field which differ in both rigs. Considering the differences in rig size and flow velocity, the relevant, energetic large scale rates of deformation (s) are larger in

our rig than in theirs and this conclusion is reached assuming for simplicity that the fluids are Newtonian and following the arguments in Section 4.2.2 of Oliveira and Pinho (1998). For this estimate s can be either an area-average value of the rate of deformation or its maximum value near the wall. In either case Oliveira and Pinho (1998) arrived at expressions of $sD/U = g(f, Re)$, so that for the same Reynolds number one obtains the same friction factor and consequently $s_{EP} = s/8$. Alternatively, we could also conclude that s is larger in our rig than in Escudier and Presti's by equating the inviscid estimate of the rate of dissipation of turbulent kinetic energy ($\varepsilon = u'^3/D$) with the exact expression for the area-average rate of energy dissipation ($\langle\varepsilon\rangle$)

$$\langle\varepsilon\rangle = \frac{4U\tau_w}{\rho D} \tag{11}$$

to arrive at a ratio of the typical fluctuating velocities in the two rigs of $u' \approx 2u'_{EP}$. This result is identical to the ratio of bulk velocities and, the similar values of u'/U measured in both rigs with the laponite suspensions and water suggest that the addition of the clay will not change dramatically the above order of magnitude estimates. Now, the higher values of the fluctuating velocity in the smaller diameter pipe implies larger rates of deformation, i.e., since $s \approx u'/D, s_{EP} \approx s/8$.

It is difficult to ascertain whether our more violent turbulent flow will compensate for our shorter transit time in the destruction of the internal structure, but what is clear is that the true viscosity in the wall region must be significantly higher than that determined exclusively on the basis of the wall shear stress and the rheogram. Had we measured the velocity profiles for all flow conditions, in order to quantify accurately the existing wall shear rate, the $f - Re$ data in Fig. 5 would be shifted to the left and drag reduction would then be observed.

This was attempted but, unfortunately, our LDA measurements did not have the spatial accuracy required to obtain measurements within the laminar sublayer. The exception was one test with the 1% laponite at $Re_w = 37,200$ and less so for the $Re_w = 61,030$ test with 1.5% laponite (here the nearest point to the wall was located at $y^+ \approx 23$). The corresponding drag reduction results, where the wall viscosity is calculated either from the flow curve and measured shear stress or from the ratio of the measured wall stress to the measured wall shear rate, are compared in Table 6. The data in Table 6 pertains to cases above the critical Reynolds number for the crossover of DR and DR_v in Fig. 6.

The data on the left-half of the table shows that DR_v exceeds the total DR, but those on the right-half tell a different story. By using the true wall viscosity, calculated from the ratio of the measured wall shear stress to the wall shear rate measured with LDA, the anomalous behaviour disappears, i.e., now $DR_v < DR$ and the drag reduction with the 1.5% suspension exceeds that of the 1% suspension. However, for the 1.5% laponite the magnitude of drag reduction is still small and well below that of Escudier and Presti for the same 1.5% suspension. Note, however, that for this fluid our measurement of wall shear rate by LDA is not correct because the point nearer to the wall is well within the buffer layer. For polymer solutions, it is well known that a decrease in pipe diameter increases drag reduction by shifting the $f - Re$ curve down and to the left provided the drag reductions are below the maximum, but here the opposite trend is observed with the two sets of 1.5% laponite data.

We should be aware that on the right column of Table 6 the wall Reynolds number is estimated with the true wall viscosity, but the value of n used in Eq. (3) is still that from the equilibrium flow curve and not the value corresponding to the equilibrium condition in the pipe flow rig. We do not expect this factor to be dramatically influent as the equilibrium affects the whole viscosity curve.

In any case, it is clear from our measurements and using our normalisation that for the pure laponite suspensions at high Reynolds numbers the friction factor did not differ significantly from the Newtonian data in contrast to what happens with the blend or with pure polymer solutions (see Escudier et al., 1992). It is also clear that the differences relative to the measurements of Escudier and Presti (1996) for 1.5% laponite are rather large and need to be clarified in future work.

4.3. Detailed velocity characteristics

Mean and turbulent velocities were measured for a series of flow conditions of the various fluids investigated above. Fig. 7 shows transverse plots of the mean axial velocity in wall co-ordinates. The plot includes data for a water flow at $Re = 50,000$ and the full line represents the Newtonian laminar sublayer, the log-law

Table 6
Effect of the wall viscosity on drag reduction effectiveness

Fluid	f	η_w from equilibrium flow curve			$\eta_w = \tau_{w,meas}/\dot{\gamma}_{w,meas}$		
		Re_w	DR (%)	DR_v (%)	Re_w	DR (%)	DR_v (%)
1% Lap	0.02149	37,200	4.5	5.4	33,200	6.3	5.0
1.5% Lap	0.02051	58,970	0.6	6.3	39,100	7.2	4.9

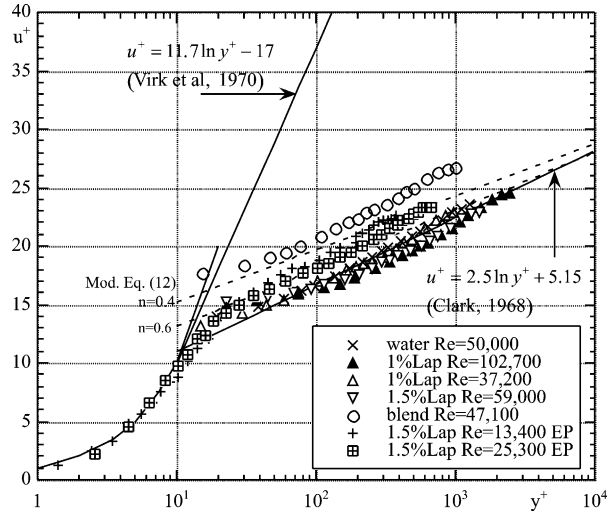

Fig. 7. Profiles of the mean axial velocity in wall coordinates. EP refers to data from Escudier and Presti (1996).

of Clark (1968) and Virk's maximum drag reduction asymptote (Virk et al., 1970). The two dashed lines are from a modification of the log-law profile for purely viscous shear-thinning fluids derived by Dodge and Metzner (1959), but correctly presented by Skelland (1967), [1] for values of n equal to 0.4 and 0.6. That equation is

$$u^+ = 2.457n^{0.25}\ln y^+ - \frac{0.566}{n^{1.2}} + \frac{2.475}{n^{0.75}} \times \left[1.960 + 0.816n - 1.628\log_{10}\left(3 + \frac{1}{n}\right)\right] \qquad (12)$$

and the modification plotted in the figure was simply the substitution of coefficients 2.457 by 2.5 in order to give Clark's expression when $n = 1$. The figure includes two profiles for 1.5% laponite from Escudier and Presti (1996).

The figure shows the good agreement of the Newtonian data with Clark's log-law equation. The data for the blend is positively deviated from Clark's log-law in agreement with the observed drag reduction. The two profiles from Escudier and Presti are positively shifted from the Newtonian log-law by an amount which is less than that shown by the clay–polymer blend which is also consistent with the friction factor data plotted in Fig. 6. There, the blend had a higher amount of drag reduction than the 1.5% pure suspension of Escudier and Presti (EP). However, for our flows with the 1.5% and the 1% laponite suspensions at the highest Reynolds number the data are slightly below Clark's law and there are two possible reasons: a higher wall shear stress, and so a true condition of drag increase, or the true viscosity is larger than the value used here to calculate y^+ as discussed in the previous section. Looking at Table 6, and accepting its right-hand side data for the 1.5% laponite suspension, the true viscosity in the pipe flow would be 33% larger than that given by the rheogram and this amount would be sufficient to shift the corresponding $y^+ - u^+$ data in Fig. 7 to the left and eliminate the inconsistency. Anyway, and as mentioned in the previous section regarding the $f - Re$ plot, this shift would not be sufficient to make our 1.5% laponite velocity data to coincide with that of Escudier and Presti for the same nominal fluid.

For each flow condition, the data closest to the wall in Fig. 7 has a tendency to deviate upwards as a consequence of mean gradient broadening for which the data was not corrected, as stated in Section 2.2.

The corresponding transverse profiles of the rms of the instantaneous axial, tangential and radial velocities are plotted in Figs. 8(b), 9(b), and 10(b), respectively. The velocity data have been normalised by the centreline velocity U_0 and in Figs. 8(a), 9(a), and 10(a) the Newtonian data are compared with the literature. The Newtonian data have been normalised with the friction velocity since that was how the data were available in the literature. For the presentation of our results and those of Escudier and Presti we preferred to normalise with the centreline velocity to enhance some effects. The Newtonian profiles compare well with the literature data and the non-Newtonian profiles are not too different from those of the water measurements. For the pure suspension flows at high Reynolds numbers this is consistent with purely viscous behaviour with practically no drag reduction.

However, this picture differs again from that conveyed by Escudier and Presti's data and there is also a discrepancy with our blend data. For the axial component of turbulence EPs data tends to increase above ours in the wall region, but the difference is small. This is typical of fluids exhibiting drag reduction which have axial turbulent velocities similar to those of Newtonian fluids in the pipe core but higher near the wall and, when normalised with the friction velocity the higher wall axial turbulence is further enhanced. The latter is also observed, but to a lesser extent, by our blend data when u' is normalised with the friction velocity, not shown here for reasons of space.

In both transverse directions, and especially so in the radial direction, EP's turbulence is strongly attenuated, whereas in the case of our more drag reducing blend the attenuation of transverse turbulence is either absent or just starting. Plots of w'/u^* and v'/u^* would have shown that the blend data lie just above the other laponite and water data, and that the w'/u^* profile for the 1.5% laponite suspension of EP, on the contrary, would be already below our measurements. Even with the friction velocity as the reference velocity, the remaining

[1] In the original paper, Dodge and Metzner (1959), the log-law for purely viscous power law fluids is wrong as pointed out by Skelland (1967).

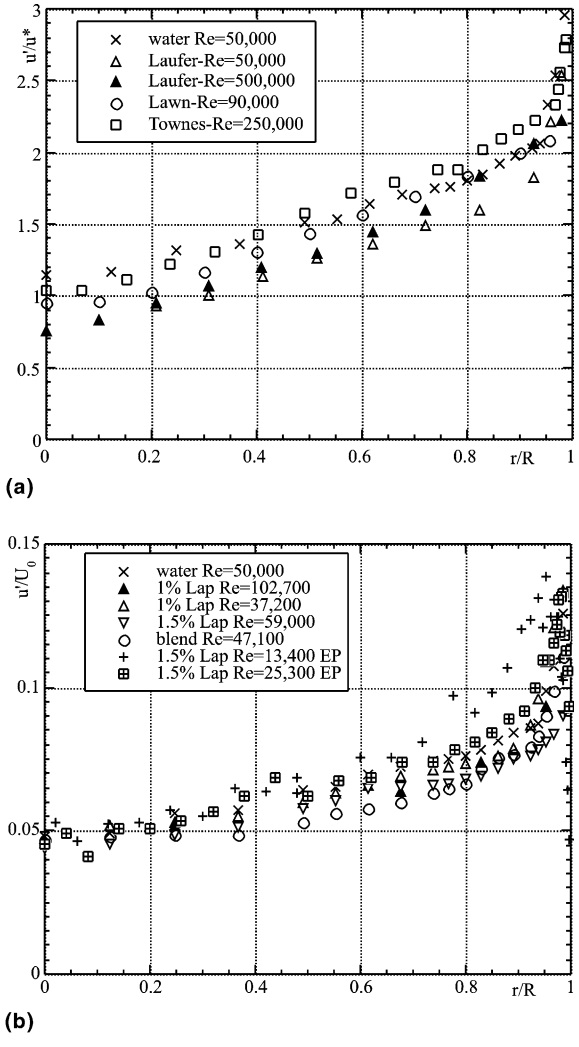

Fig. 8. Rms of the fluctuations of the axial component of turbulence in pipe flow. (a) Comparison between the water measurements and data from literature: Laufer (1954), Lawn (1971), Townes et al. (1972); (b) comparison between measurements with water and laponite-based fluids. EP refers to data from Escudier and Presti (1996).

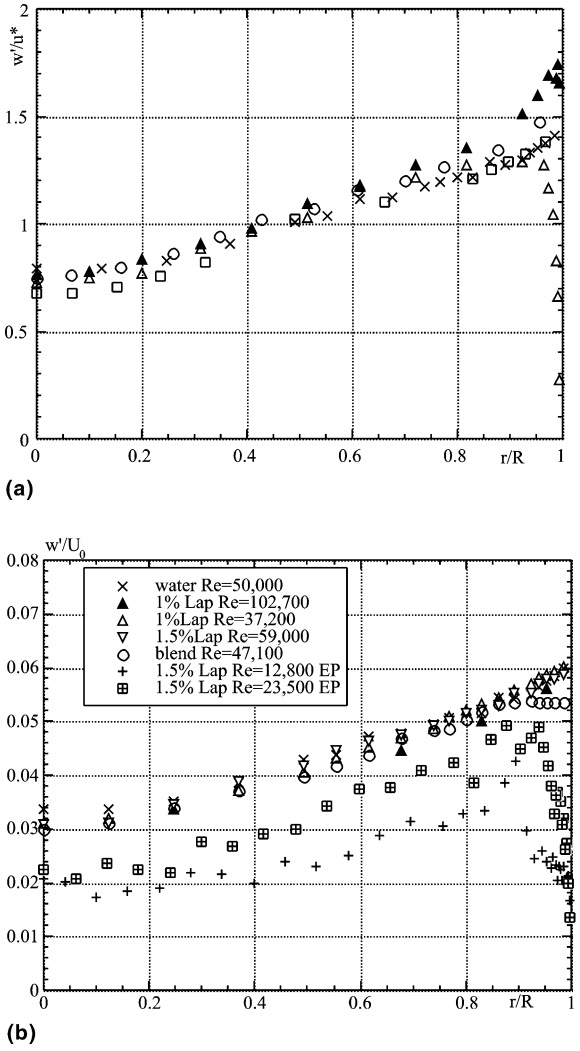

Fig. 9. Rms of the fluctuations of the tangential component of turbulence in pipe flow. Caption as in Fig. 8.

transverse turbulent profiles (v') from EP are strongly dampened.

It has been reported in the literature on turbulent duct flows of polymer solutions that drag reduction is accompanied by an increase in the peak streamwise turbulence in the wall region to values higher than those of Newtonian fluids and, at the same time, a strong dampening of the two transverse turbulent components. This has been observed experimentally by Pinho and Whitelaw (1990) and Escudier et al. (1992), and has also been found in various DNS and pseudo-DNS calculations of the turbulent channel flow, such as those of Sureshkumar et al. (1997) using the FENE-P model, and the works of Den Toonder et al. (1995) and Orlandi (1995). The higher peak in the longitudinal turbulence was observed experimentally only for high drag reduction intensities, but the attenuation of transverse turbulence is almost always present. This refers to turbulent velocities normalised by the bulk or centreline velocities. If the friction velocity is used to scale data, enhancement of longitudinal turbulence and attenuation of transverse turbulence is already observed with moderate drag reduction intensities. Such features are not seen here, especially with the drag reducing laponite/CMC blend, but were again observed by Escudier and Presti (1996) with pure laponite suspensions of the same clay, at the same 1.5% concentration. With the blend there is a decrease of the maxima of tangential and radial turbulence relative to that of the other fluids, but the difference is rather small.

This is an important finding because it suggests a drag reduction mechanism for thixotropic suspensions, in particular for the blend, which is different from that seen with time-independent elastic polymer solutions. In fact, whereas with polymer solutions DR is usually associated with the interaction between turbulence and the molecular conformation, affecting its rheological properties,

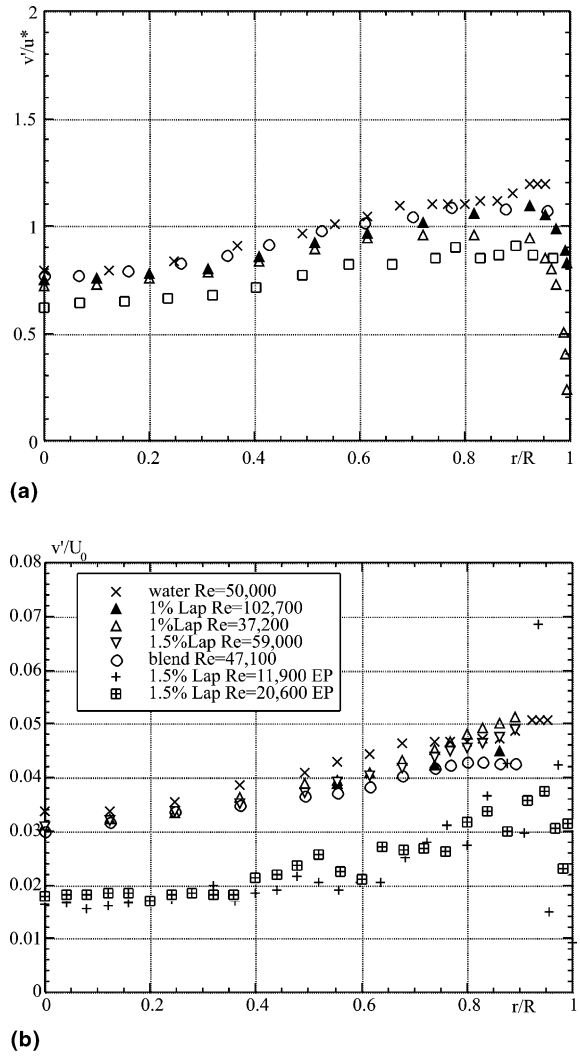

Fig. 10. Rms of the fluctuations of the radial component of turbulence in pipe flow. Caption as in Fig. 8.

and in particular its elongational viscosity, in the case of suspensions one of the mechanisms of drag reduction can be particle migration from the wall, see Lumley (1978).

Another mechanism of drag reduction in suspensions is related to the effect of the particles in suppressing radial turbulent movement of the fluid, but there is also an increase of radial momentum transfer due to inter-particle contact. With suspensions of elongated particles drag reduction results from the predominance of the first over the second mechanism and is thus limited to a range of concentrations, as investigated by Kerekes and Douglas (1972) assuming purely viscous behaviour. At large particle concentrations the motion of the particles is strongly inhibited and the fluid acquires an yield stress, as in here, and drag reduction is no longer observed, at least as a mechanism purely attributed to viscometric viscosity effects. The end of this purely viscous drag reduction mechanism depends of fluid composition and could co-exist, in some cases, with small values of yield stress but there could also be particle migration from the wall or the suppression of radial transfer of momentum by the action of a property other than the viscometric viscosity. Particle migration seems unlikely, at least for the pure suspensions, because the Reynolds numbers for these submicron sized particles in the wall region, and based on the particle relative velocity, are well within the Stokes flow regime.

Could it be that particle migration is being more effective with the blend than with the more concentrated, but pure, clay suspensions? Polymer molecules stick to particles and increase their effective size and asymmetry, thus raising the particle Reynolds number and the likelihood of migration effects. The formation of a low viscosity lubricating layer of fluid would give rise to drag reduction, but have only a minimal effect upon the turbulent profiles normalised by the centreline or bulk velocities as in here, which tend to be affected mainly by the Reynolds number. Then, the question is: why is the picture shown by Escudier and Presti, for pure laponite, similar to that seen with pure polymer solutions? The difference between ours and EP's 1.5% laponite suspension is the age of the fluid, with their suspension being older and more viscous. Aging results in the formation of larger platelets, but not as large as those that result from the interaction of clay particles with polymer molecules, so particle migration is unlikely to be the cause for DR with the aged pure suspensions and here the mechanism must be another one, relating fluid properties (such as elongational viscosity or viscosity anisotropy) with internal structure of the clay suspension.

What we must conclude is that for both thixotropic fluids, the pure clay suspension and the clay-polymer blend, there is really a very complex interaction between the internal structure of the fluid, its age and rheology and the resulting hydrodynamic behaviour and this needs to be further investigated. It is also clear that any future work on this subject should use advanced diagnostic techniques that are spatially accurate to measure directly the wall shear rate and remove the ambiguity regarding the quantification of the wall viscosity.

5. Conclusions

A detailed investigation of the rheology and turbulent pipe flow characteristics of clay suspensions and one clay–polymer blend was carried out. The clay suspensions were based on laponite RD from Laporte Industries at weight concentrations of 1% and 1.5% and the blend was made of 0.5%/0.07% by weight laponite/CMC 7H4C (from Hercules).

The fluids were shear-thinning and thixotropic, so the measurement of the viscometric viscosity had to follow an equilibrium procedure. The fluids exhibited yield stress which was measured by two direct methods and a curve fitting procedure. The yield stress values were of around 0.9, 2.1 and 3.4 Pa for the 1% laponite, the blend and the 1.5% laponite fluids, respectively. The oscillatory shear flow test showed that the 1% laponite suspension was almost inelastic, whereas the 1.5% laponite and the blend exhibited some elasticity. In particular, the blend exhibited a strong synergetic effect in that the levels of viscosity and of elasticity were far higher than for the isolated additives and of similar magnitude as for the more concentrated suspensions.

The turbulent pipe flow measurements confirmed the findings of Escudier and Presti (1996), that the true wall viscosity in the pipe is higher than that obtained through the rheogram, and showed only a small amount of drag reduction for the pure laponite suspensions, which basically results from shear-thinning behaviour at Reynolds numbers in excess of 35,000. The detailed mean and turbulent velocity measurements confirmed this picture by showing profiles similar to those of water. However, for the polymer–clay blend there was clearly drag reduction. The results were compared with those of Escudier and Presti (1996) for a pure 1.5% laponite suspension, which showed significant drag reduction, and the possible causes for the observed discrepancies were discussed. Further research needs to be conducted in order to explain the discrepancies observed in this and the work of Escudier and Presti (1996).

Acknowledgements

The authors acknowledge the financial support of the Stichting Fund of Schlumberger. The laboratory facilities provided by INEGI – Instituto de Engenharia Mecânica e Gestão Industrial – were fundamental for the successful outcome of this work and the helpful discussions with Prof. M.P. Escudier, University of Liverpool, helped to clarify many issues.

References

Alderman, N.J., Ram Babu, D., Hughes, T.L., Maitland, G.C., 1988. The rheological properties of water-based drilling fluids. In: Proceedings of Xth International Congress on Rheology, Sydney, pp. 140–142.

Barnes, H.A., Hutton, J.F., Walters, K., 1989. An Introduction to Rheology. Elsevier, Amsterdam.

Barnes, H.A., 2000. A Handbook of Elementary Rheology. Institute of Non-Newtonian Fluid Mechanics, University of Wales, Aberystwyth.

Boger, D.V., 1994. Rheology of suspensions. Lecture Series 1994-03, Non-Newtonian Fluid Mechanics, Von Kárman Institute for Fluid Dynamics.

Casson, W., 1959. A flow equation for pigment-oil suspensions of the printing ink type. In: Mill, C.C. (Ed.), Rheology of Dispersed Systems. Pergamon, Oxford, p. 84.

Charm, S.E., 1963. Effect of yield stress on the power law constant of fluid food materials determined in low shear rate viscometers. Ind. Eng. Chem., Process Des. Dev. 2, 62–65.

Cheng, D.C.-H., 1984. Further observations on rheological behaviour of dense suspensions. Powder Technol. 37, 255–273.

Cheng, D.C.-H., 1986. Yield Stress: a time-dependent property and how to measure it. Rheol. Acta 25, 542–554.

Clark, J.A., 1968. A study of incompressible turbulent boundary layers in channel flow. J. Basic Eng. 90, 455–468.

Cocard, S., Nicolai, T., Tassin, J.-F., 2000. Thixotropic behaviour of laponite suspensions as studied by rheo–optical techniques. In: Proceedings of the XIIIth International Congress on Rheology, Cambridge, UK, vol. 4, pp. 160–162.

Coelho, P.M., Pinho, F.T., 1998. Comportamento reológico de algumas soluções aquosas diluídas de polímero. Mecânica Exp. 3, 51–61.

Toonder, J.M.J., Nieuwstadt, F.T.M., Kuiken, G.D.C., 1995. The role of elongational viscosity in the mechanism of drag reduction by polymer additives. Appl. Sci. Res. 54, 95–123.

Dodge, D.W., Metzner, A.B., 1959. Turbulent flow of non-Newtonian systems. AIChE J. 5, 189–204.

Durst, F., Melling, A., Whitelaw, J.H., 1981. Principles and Practice of Laser-Doppler Anemometry, second ed. Academic Press, New York.

Escudier, M.P., Jones, D.M., Gouldson, I.W., 1992. Fully developed pipe flow of shear-thinning liquids. In: Sixth International Symposium on Applications of Laser Techniques to Fluid Mechanics, Lisbon, paper 1.3.

Escudier, M.P., Gouldson, I.W., Jones, D.M., 1995a. Taylor vortices in Newtonian and shear-thinning liquids. In: Proc. R. Soc. London A, vol. 449, pp. 155–176.

Escudier, M.P., Gouldson, I.W., Jones, D.M., 1995b. Flow of shear-thinning fluids in a concentric annulus. Exp. Fluids 18, 225–238.

Escudier, M.P., Presti, F., 1996. Pipe flow of a thixotropic liquid. J. Non-Newt. Fluid Mech. 62, 291–306.

Escudier, M.P., Gouldson, I., Pereira, A.S., Pinho, F.T., Poole, R.J., 2001. On the reproducibility of the rheology of shear-thinning liquids. J. Non-Newt. Fluid Mech. 97, 99–124.

Franklin, R.E., Wallace, J.M., 1970. Absolute measurements of static-hole error using flush transducers. J. Fluid Mech. 42, 33–48.

Geiringer, P.L., 1963. High Temperature Water Heating. Wiley, New York.

Iwamiya, J.H., Chow, A.W., Sinton, S.W., 1994. NMR flow imaging of Newtonian liquids and a concentrated suspension through an axisymmetric sudden contraction. Rheol. Acta 33, 267–282.

Keentok, M., 1982. The measurement of yield stress of liquids. Rheol. Acta 21, 325–332.

Kerekes, R.J.E., Douglas, W.J.M., 1972. Viscosity properties of suspensions at the limiting conditions for turbulent drag reduction. Can. J. Chem. Eng. 50, 228–231.

Laponite, 1979. Laponite/polymer interactions. Laponite Technical Bulletin L61, Laporte Absorbents, Cheshire, UK.

Laponite, 1980. Laponite: structure, properties and relationship to natural clays. Laponite Technical Bulletin L64, Laporte Absorbents, Cheshire, UK.

Laponite, 1990a. Laponite Technical Bulletin L106/90/C, Laporte Inorganics, Cheshire, UK.

Laponite, 1990b. Laponite-Structure, chemistry and relationship to natural clays. Laponite Technical Bulletin L104/90/A, Laporte Absorbents, Cheshire, UK.

Laufer, J., 1954. The structure of turbulence in fully developed pipe flow. NACA report 1174.

Lawn, C.J., 1971. The determination of the rate of dissipation in turbulent pipe flow. J. Fluid Mech. 48, 477–505.

Liddell, P.V., Boger, D.V., 1996. Yield stress measurements with the vane. J. Non-Newt. Fluid Mech. 63, 253–261.

Lockett, T.J., 1992. Numerical simulation of inelastic non-Newtonian fluid flows in annuli, Ph.D. Thesis, Imperial College, University of London.

Lumley, J.L., 1978. Two-phase and non-Newtonian flows. In: Bradshaw, P. (Ed.), Turbulence. Springer, Berlin, pp. 289–324 (Chapter 7).

Mewis, J., 1979. Thixotropy – a general review. J. Non-Newt. Fluid Mech. 6, 1–20.

Nguyen, Q.D., Boger, D.V., 1983. Yield stress measurement for concentrated suspensions. J. Rheol. 27, 321–349.

Nguyen, Q.D., Boger, D.V., 1992. Measuring the flow properties of yield stress fluids. Ann. Rev. Fluid Mech. 24, 47–88.

Novotny, E.J., Eckert, R.E., 1973. Direct measurement of hole error for viscoelastic fluids in flow between infinite parallel plates. Trans. Soc. Rheol. 17, 227–241.

Oliveira, P.J., Pinho, F.T., 1998. A qualitative assessment of the role of a viscosity depending on the third invariant of the rate-of-deformation tensor upon turbulent non-Newtonian flow. J. Non-Newt. Fluid Mech. 78, 1–25.

Orlandi, P., 1995. A tentative approach to the direct simulation of drag reduction by polymers. J. Non-Newt. Fluid Mech. 60, 277–301.

Papenhuijzen, J.M.P., 1972. The role of particle interactions in the rheology of dispersed systems. Rheol. Acta 11, 73–88.

Park, J.T., Mannheimer, R.T., Grimley, T.A., Morrow, T.B., 1989. Pipe flow measurements of a transparent non-Newtonian slurry. ASME J. Fluids Eng. 111, 331–336.

Pereira, A.S., 2000. Flow of non-Newtonian fluids through sudden expansions (in Portuguese), Ph.D Thesis, University of Porto, Portugal.

Pereira, A.S., Pinho, F.T., 1994. Turbulent pipe flow characteristics of low molecular weight polymer solutions. J. Non-Newt. Fluid Mech. 55, 321–344.

Pereira, A.S., Pinho, F.T., 1999. Reologia de suspensões tixotrópicas de base argilosa (laponite). Mecânica Exp. 4, 51–63.

Pinho, F.T., Whitelaw, J.H., 1990. Flow of non-Newtonian fluids in a pipe. J. Non-Newt. Fluid Mech. 34, 129–144.

Pryce-Jones, J., 1952. Studies in thixotropy. Kolloid–Z. 126, 96–122.

Shah, V.L., 1980. Blood flow. In: Mujumdar, A.S., Mashelkar, R.A. (Eds.), Advances in Transport Processes, vol. 1. Wiley Eastern Limited, New Delhi.

Shaw, R., 1960. The influence of hole dimensions on static pressure measurements. J. Fluid Mech. 7, 550–564.

Skelland, A.H.P., 1967. Non-Newtonian Flow and Heat Transfer. Wiley, New York.

Speers, R.A., Hilme, K.R., Tung, M.A., Williamson, W.T., 1987. Drilling fluid shear stress overshoot behavior. Rheol. Acta 26, 447–452.

Stieglmeier, M., Tropea, C., 1992. A miniaturized, mobile laser-Doppler anemometer. Appl. Opt. 31, 4096.

Sureshkumar, R., Beris, A.N., Handler, R.A., 1997. Direct numerical simulation of the turbulent channel flow of a polymer solution. Phys. Fluids 9, 743–755.

Townes, H.W., Gow, J.L., Powe, R.E., Weber, N., 1972. Turbulent flow in smooth and rough pipes. J. Basic Eng. 94, 353–362.

Virk, P.S., Mickley, H.S., Smith, K.A., 1970. The ultimate asymptote and mean flow structure in Tom's phenomena. J. Appl. Mech. 92, 488–493.